Advances in Military Technology
Vol. 17, No. 2, 2022, pp. 163-177
ISSN 1802-2308, eISSN 2533-4123
DOI 10.3849/aimt.01525

Numerical Modelling of Discharging the Lithium-Sulphur Batteries in Ansys Fluent

M. Mačák,[1] P. Vyroubal,[1*] T. Kazda,[1] D. Capková[2] and J. Maxa[1]

[1] *Department of Electrical and Electronic Technology, Faculty of Electrical Engineering and Communication, Brno University of Technology, Czech Republic*
[2] *Department of Physical Chemistry, Faculty of Sciences, Pavol Jozef Šafárik University in Košice, Slovak Republic*

The manuscript was received on 13 August 2021 and was accepted after revision for publication as research paper on 25 August 2022.

Abstract:

Lithium-sulphur batteries appear to be an exciting technology for energy storage. This technology could be used in aviation, aerospace or in heavy electric vehicles, or even for mobile applications. This article deals with the implementation of a modified Li-S battery charging and discharging model, specifically in the MSMD module, which does not have this model by default. The behavior of the new model was tested experimentally on a real Li-S battery and the results were compared with simulations, which gave very good and consistent results. Compared to commonly used equivalent circuit models, MSMD is able to study macroscopic effects such as electric potential distribution or temperature distribution in the battery, while the simulation remains simple, fast and accurate.

Keywords:

equivalent circuit model, Multi-Scale Multi-Domain, lithium-sulphur battery, numerical simulation

1 Introduction

The reliability of energy source is a very important factor for any military application. Fossil fuels currently used in the military have high costs attached to them, as it is also necessary to consider their transport to remote locations. Additionally, it results in a considerable vulnerability to the logistic sector.

To ensure safe and secure energy source, military bases around the world are developing stationary battery storage systems coupled with renewable energy sources

* *Corresponding author: Department of Electrical and Electronic Technology, FEEC, Brno University of Technology, Technická 10, CZ-616 00 Brno, Czech Republic. Phone: +420 541 14 61 49, E-mail: vyroubal@vut.cz. ORCID 0000-0003-4160-803.*

such as wind or solar. These systems can provide immediate, flexible, and clean power in case of energy or logistic disruption [1].

Additionally, the ever-expanding introduction of electric vehicles is also receiving more attention in the military area, especially due to their better fuel economy and lower pollution emission. Electric motors can be also built directly inside the wheels, which can increase the acceleration and the maneuverability. These vehicles can also act as a mobile power generator capable of producing significant amount of electricity. Unfortunately, a widespread introduction of these systems is inhibited by the technology of current Li-Ion batteries as they have often insufficient parameters, such as low energy density, heavy weight, or long charging times [2].

Lithium-sulphur (Li-S) cells have a great premise to become a prominent next generation energy storage technology. Their advantage lies in their significant theoretical energy density (2 600 $W \cdot h \cdot kg^{-1}$) and capacity (1 675 $mA \cdot h \cdot g^{-1}$). Sulphur also does not harm the environment and its production is not expensive due to its abundance [3]. In recent years, a huge amount of progress has been made in the enhancing of Li-S battery parameters [4].

Their favorable properties make them an excellent candidate in various military applications. The low weight, high energy density and high safety of the Li-S batteries is especially important for aviation or aerospace. Their low weight can lead to a decrease in weight and size of drones or aircrafts, which would ensure higher flight ranges. This technology might also find its place in heavy electric vehicles. Reduced battery weight would increase range and payload, which would allow to travel longer distances between charging. This is especially important for locations with difficult terrain, where the charging infrastructure might not be viable. Their light weight is also favorable for mobile operations, as soldiers (thermal vision, lights, medical equipment) would not need to carry heavier Li-Ion batteries [5, 6].

However, the real-life application of Li-S technology is slowed down by complicated dissolution/precipitation and electrochemical reactions between a considerable number of intermediate compounds, which can result in the decrease of the effective surface of the electrodes. In addition, elemental sulphur, as well as the end product Li_2S, are poor electrical conductors, so the conductivity of the electrodes has to be increased by applying additives such as carbon [3, 4].

To accelerate the practical implementation of Li-S batteries, establishing an appropriate numerical model is necessary. While the experimental research is considerably profound, the application of computational models is not very widespread. There are two main approaches in numerical modelling: 1D physics-based electrochemical models and 0D equivalent circuit models (ECMs) [7].

Due to the complexity of electrochemical models, ECMs pose as a suitable alternative. While considerably simpler, they retain their accuracy, which is very important for real life applications, as it is often not necessary to resolve internal physical behavior of the battery. The ECMs are created by combining different circuit elements such as resistors, capacitors, constant phase elements, Warburg impedance elements, and voltage sources. The imperfect characteristics of a battery are modelled with constant phase elements and Warburg impedance elements, which offer higher precision of the description. In practice, they are often approximated with a resistor and a capacitor connected parallelly (R-C element) to reduce the computational complexity [8, 9]. Generally, the Li-S ECMs consist of a serial resistor connected to a few R-C elements [10]. The component values are extracted from electrochemical impedance spectroscopy or current pulse measurements [11]. In the literature, the structure of used ECMs

slightly varied but generally consisted of a serial resistor and from one to four R-C elements [9, 10, 12, 13]. All of these studies used a custom 0D models.

This work investigates the possibility of using a commercially available software Ansys Fluent for the modelling of next-generation Li-S batteries. A 3D model of a Li-S battery was made using the Multi-Scale Multi-Domain battery module. Simulations of discharge characteristics have been carried out with different ECM parameter definitions, which were originally defined for the modelling of Li-ion batteries. The ECM parameter values were obtained from the work of Fotouhi et al. [9], which used a 3.4 Ah Li-S battery from OXIS Energy. Also, a 0D MATLAB model has been developed to evaluate and compare the differences of the 3D MSMD model. The main advantage of Ansys Fluent lies in readily available 3D computational domain and in coupling of all available physical models (hydrodynamics, heat transport, electrochemistry, electromagnetics). As a result, it would be possible to obtain complex data and overview of the battery, which is often problematic or even impossible to acquire experimentally or with stand-alone ECMs.

2 Numerical Model

The presented model was built using the Dual Potential Multi-Scale Multi-Domain (MSMD) model fully implemented in the Computational Fluid Dynamics (CFD) software Ansys Fluent, which uses finite volume method to solve partial differential equations. The MSMD model overcomes the necessity of completely resolving the geometry of the battery (current collector, electrodes, and separators) by treating the battery as an orthotropic continuum. The battery is then divided into three parts: active zone (cell body), positive tab and negative tab. As a result, the computational mesh is not constrained by the micro-structure of the battery. Different physical phenomena can be then separated by their length scales. Large scale phenomena such as electric potential and temperature distribution on each current collector are resolved by a coarse CFD mesh at the battery's geometry scale, while the electrochemical reactions are only solved locally. The following equations are solved in the battery active zone [14-16]:

$$\nabla \cdot \left(\sigma_{+} \nabla \varphi_{+} \right) = -J \tag{1}$$

$$\nabla \cdot \left(\sigma_{-} \nabla \varphi_{-} \right) = +J \tag{2}$$

$$\frac{\partial \rho c_{\mathrm{p}} T}{\partial t} - \nabla \cdot \left(k \nabla T \right) = \sigma_{+} \left| \nabla \varphi_{+} \right|^2 + \sigma_{-} \left| \nabla \varphi_{-} \right|^2 + S_{\mathrm{E}} \tag{3}$$

where σ_{+} and σ_{-} [S·m^{-1}] are the effective electric conductivity of the positive and the negative electrode, φ_{+} and φ_{-} [V] are the phase potentials for the positive and negative electrodes, J [A·m^{-3}] describes the volumetric current density caused by electrochemical reactions, S_{E} [W·m^{-3}] describes heat source term caused by electrochemical reactions, ρ [kg·m^{-3}] is the battery effective density, c_{p} is the specific heat capacity [J·kg^{-1}·K^{-1}], and k is the thermal conductivity [W·m^{-1}·K^{-1}].

2.1 Electrochemical Sub-Model

Electrochemical sub-models describe the battery characteristics and relate the local current density to the volumetric current density source term in the macroscopic equa-

tions. The electrochemical behavior of the studied Li-S battery was described by an Equivalent Circuit Model, which is fully supported by Ansys Fluent. This sub-model was based on the work of Chen and Rincon-Mora [17], in which the battery behavior is mimicked by a 2 R-C electrical circuit, which consists of three resistors and two capacitors as shown in Fig. 1.

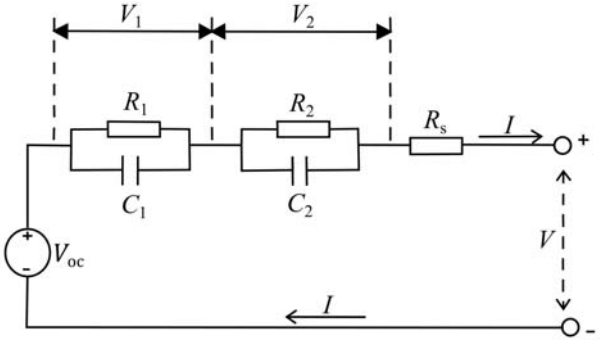

Fig. 1 Illustration of 2 R-C ECM used in Ansys Fluent [16]

The local cell voltage can be calculated from a set of differential algebraic equations [17, 18]:

$$V = V_{\mathrm{OC}} + V_1 + V_2 - R_S \cdot I \tag{4}$$

$$\frac{\mathrm{d}V_1}{\mathrm{d}t} = -\frac{1}{R_1 C_1} V_1 - \frac{1}{C_1} I \tag{5}$$

$$\frac{\mathrm{d}SoC}{\mathrm{d}t} = \frac{I}{3\,600Q} \tag{6}$$

where V is the cell voltage [V], V_{OC} is the open circuit voltage [V], V_1 [V] and V_2 [V] are the voltages at the R-C elements, R [Ω] is the resistance of a resistor, C [F] is the capacitance of a capacitor, I [A] is the charging or discharging current, Q [Ah] is the battery capacity and SoC is the State of Charge.

The V_{OC}, resistances and capacitances are functions of the battery SoC. Ansys Fluent offers different definitions of the circuit parameters dependency on the battery SoC.

The first description of the parameters is based on the work of Chen and Rincon-Mora [17]:

$$X_{\mathrm{RC}} = b_0 + b_1 \cdot \exp\left(-b_2 \cdot SoC\right) \tag{7}$$

$$V_{\mathrm{OC}} = c_0 + c_1 \cdot SoC + c_2 \cdot SoC^2 + c_3 \cdot SoC^3 + c_4 \cdot \exp\left(-c_5 \cdot SoC\right) \tag{8}$$

where X_{RC} describes any R or C element, b and c are the constant coefficients [–] and V_{OCV} [V] is the open circuit voltage.

The second description uses a 5$^{\mathrm{th}}$ order polynomial equation:

$$X = a_0 + a_1 \cdot SoC + a_2 \cdot SoC^2 + a_3 \cdot SoC^3 + a_4 \cdot SoC^4 + a_5 \cdot SoC^5 \tag{9}$$

where every R and C element, as well as the open circuit voltage, is described by this equation.

Third definition uses a look-up table, which consists of the parameter values at defined SoCs. Parameter values between the table points are then linearly interpolated. This method should be able to describe even complex cases, as the values are not bound by any fitting function.

2.2 Coupling between ECM Sub-Model and Macroscopic MSMD Model

During computation, the electrochemical model is calculated for every finite volume at every timestep. Even though Eqs (1) and (2) do not contain any transient terms, they are solved in a transient manner because of the changes in the battery SoC during charge/discharge, which results in a varying current density source term. The coupling between the electrochemical ECM and the macroscopic model is based on the equality of voltage calculated by the ECM and the potential difference obtained from Eqs (1) and (2) [17, 18]:

$$V = V_{\mathrm{OC}} + V_1 + V_2 - R_{\mathrm{S}} \cdot I = \varphi_+ - \varphi_- \tag{10}$$

Thus, the potential at the resistor R_s can be defined as:

$$V_{\mathrm{S}} = V_{\mathrm{OC}} - V_1 - V_2 - \left(\varphi_+ - \varphi_-\right) \tag{11}$$

The volumetric current density at every cell, which couples the electrochemical sub-model with the macroscopic model, can be defined through the potential V_S at the series resistor R_S as [14, 15]:

$$J = \frac{V_{\mathrm{S}}}{R_{\mathrm{S}} \cdot Vol} \tag{12}$$

where Vol is the volume of the battery active zone [m^3].

3 Simulation

The numerical simulations presented in this work investigate the applicability of Ansys Fluent MSMD module for the modelling of Li-S batteries. A series of simulations with different ECM parameter definitions (Chen's definition [17], a 5th order polynomial definition and a look-up table definition) were carried out. In order to better evaluate the results, the circuit parameters were estimated from [14], in which the parameters were extracted from a 3.4 Ah Li-S battery from OXIS Energy at the temperature of 30 ºC and compared with the results from Stroe et al. [13].

Even though the equivalent circuit used in [9] consisted of only one R-C element, while Ansys Fluent uses equivalent circuit with 2 R-C elements, it was possible to fix the values of the second R-C element to zero without causing any problems during the solution or in the accuracy of the results.

Additionally, a 0D computational model has been created in MATLAB to present another point of reference and to compare the differences between the 3D MSMD model and 0D pure ECMs. The MATLAB model consisted of the same equivalent circuit described by the differential algebraic Eqs (4)-(6) along with the parameter definition Eqs (7)-(9). The equations were solved by ode15s solver, which is a variable step variable order solver based on the numerical differentiation formulas designed for solving stiff problems or DAEs. A closer description of the mathematical procedure can be found in [19] and [20].

The illustration of the computational domain is shown in Fig. 2. In this case, the geometry is mainly for the illustration of the potential distribution in the battery. The dimensions of the active zone are (100 × 100 × 10) mm.

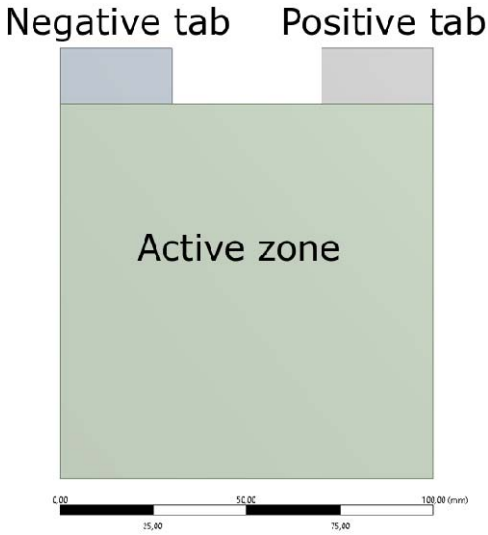

Fig. 2 Geometry of the battery used in the simulations

The simulations were carried out for a 3.4 Ah cell at a temperature of 30 ºC and for discharging current 0.1 C (0.34 A), 0.2 C (0.68 A) and 0.5 C (1.7 A). The initial *SoC* was set to 1. In these simulations the heat transport equation was not considered, as the temperature change during single discharge is minimal. The maximum and minimum voltages were set to 2.5 V and 1.5 V, respectively. The charging process was not investigated, as it is not symmetrical to the discharge. It would be necessary to extract ECM parameters during charging to properly model the charging process. All surfaces apart from the top wall of the positive tab were set as insulating (no-flux Neumann's boundary condition) for φ_+. The current rate at the top wall was defined as:

$$\frac{\partial \varphi_+}{\partial \boldsymbol{n}} = \frac{I}{A_{\text{tab}}} \tag{13}$$

where $\boldsymbol{n}$ is the normal direction vector and A_{tab} is the surface area of the top wall. The potential φ_- at the negative electrode was fixed using a Dirichlet's boundary condition of 0 V to set a reference point for the voltage distribution. Similarly, the other surfaces were set as insulating.

3.1 ECM Parameters

The values of constants for fitted functions defined by Chen and Rincon-Mora [17] and a 5$^{\text{th}}$ order polynomial were obtained through *lsqcurvefit*, which is a nonlinear least-squares solver. The data for the look-up table definition were directly estimated from [9]. The values were recorded every 0.05 SoC. The function constants for Chen's definition and for the 5$^{\text{th}}$ order polynomial are displayed in Tabs 1 and 2, respectively. Fitted functions along with data points are displayed in Fig. 3.

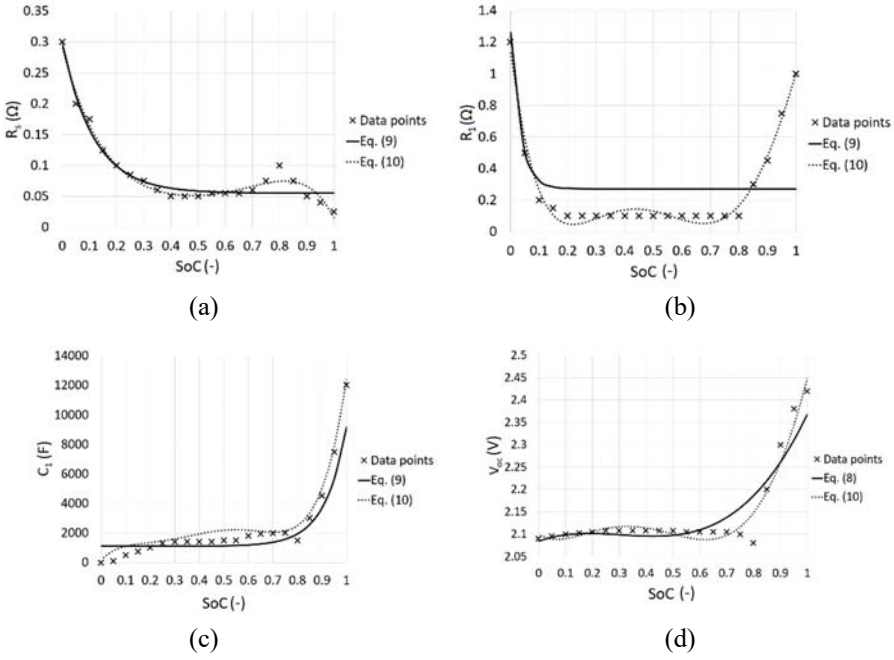

Fig. 3 Parameter functions for R_s (a), R_1 (b), C_1 (c), and Voc (d). Each figure contains data points and fitted functions (Chen's definition and the 5th order polynomial)

Tab. 1 Parameters for Chen's functions

Parameter	**Order of Coefficients**					
	0th		**1st**		**2nd**	
R_s	0.0553		0.2426		8.5404	
R_1	0.2712		0.9899		29.2337	
C_1	1102.7		0.1		−11.3	
	0th	**1st**	**2nd**	**3rd**	**4th**	**5th**
V_{OC}	16.9741	−2.9609	−0.4784	0.8646	−14.8894	0.2131

Tab. 2 Parameters for 5th order polynomial functions

Parameter	**Order of Coefficients**					
	0th	**1st**	**2nd**	**3rd**	**4th**	**5th**
R_s	0.2911	−1.6763	5.0124	−8.4648	8.0596	−3.2059
R_1	1.1395	−13.988	63.966	−127.39	112.06	−34.783
C_1	−222.76	16111	−100236	323160	−458644	231778
V_{OC}	2.0988	−0.35	3.5522	−10.142	10.505	−3.2158

For solver settings, the spatial discretization scheme for both scalars was set to first order upwind. The absolute error tolerance was set to $1 \cdot 10^{-6}$. The time steps for 0.1 C and 0.2 C were set to 50 s, for 0.5 C the time step was set to 10 s. Maximum number of iterations per timestep was set to 50. For MATLAB simulation, absolute and relative error tolerances were set to $1 \cdot 10^{-6}$.

4 Results and Discussion

4.1 Chen's Definition

The comparison between the results obtained from Ansys Fluent and MATLAB are presented in Fig. 4. It is possible to see some differences between the solutions, which are caused by a different initial solution. For MATLAB solver, the starting voltage was always 2.4 V, while the Fluent solver calculated the starting voltage based on the initial conditions. However, the main issue with this parameter definition lies in the fact that the discharge curve does not resemble the characteristic discharge shape of a Li-S battery. There is no higher voltage plateau identifying the reduction of higher chain polysulfides and no inflection point between the plateaus. The cell voltage immediately decreases exponentially from around 2.4 V to plateau situated at around 2 V for 0.1 C, which for higher discharge currents is small (1.87 V for 0.2 C) or even non-existent (0.5 C). These inaccuracies are caused by the simple parameter definition, which is suitable for Li-ion batteries, but is not suitable for batteries with more complex characteristics.

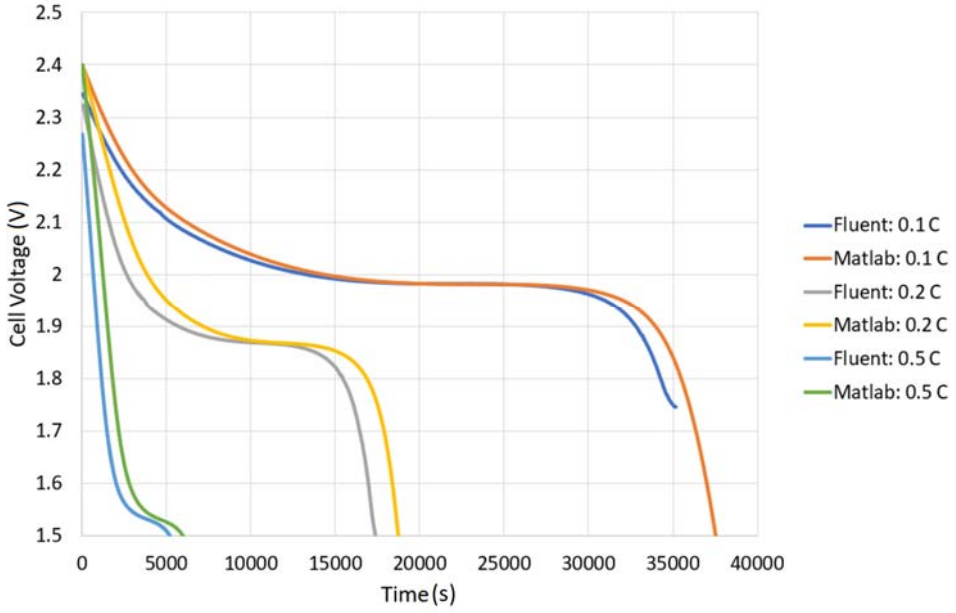

Fig. 4 Modelled discharge curves with Chen's parameter definition. The results were obtained from MATLAB and Ansys Fluent at different C-rates (0.1 C, 0.2 C and 0.5 C)

4.2 5th Order Polynomial

The comparison between the results is presented in Fig. 5. In this case, the results obtained from Ansys Fluent are in excellent agreement with the results obtained from MATLAB. It is possible to see that the 5th order polynomial function can be fitted much better than the previous functions. This results in slightly more realistic discharge curves, which exhibit traits such as long lower potential plateau and a steeper

slope at the beginning of the discharge and an inflection point between the high voltage region and the lower voltage region. However, there are a few problems such as visible oscillations, which are more prominent with the increasing C-rate. Additionally, it causes a rise of voltage near the end of the plateau. The voltage during the low potential plateau varied from 2.03 V to 2.07 V for 0.1 C. For this case, the battery at the 0 % SoC did not meet the limit of minimum 1.5 V. For the 0.2 C the voltage in the lower plateau varied from 1.98 V to 2.02 V. For the 0.5 C the voltage in the lower plateau varied from 1.78 V to 1.89 V. For both 0.2 C and 0.5 C the simulation was stopped at 1.5 V, as expected. These inaccuracies are caused by the polynomial fit, which cannot properly match the long constant set of values and creates these oscillations around data points. This is especially visible for OCV and R_1 curves (Fig. 3b, d).

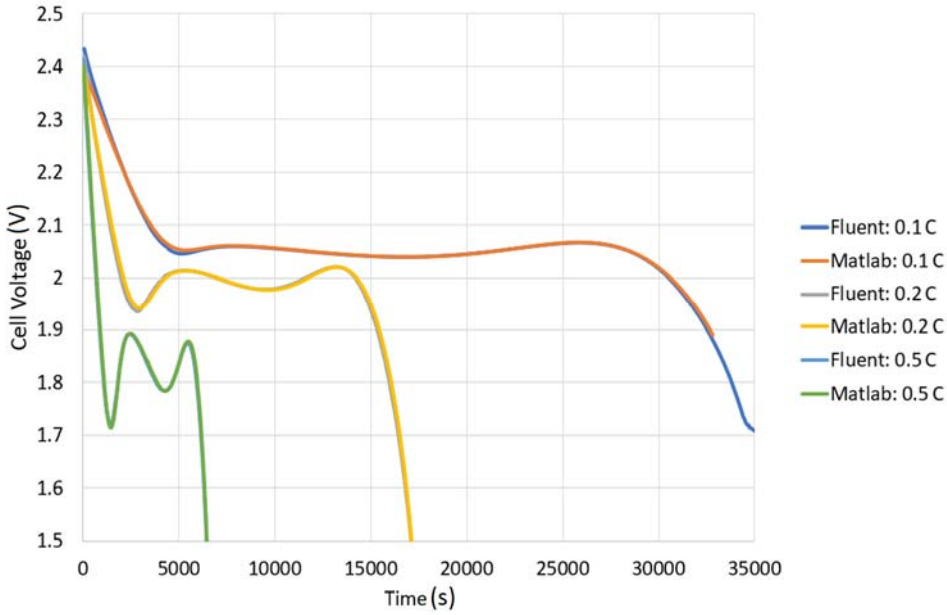

Fig. 5 Modelled discharge curves with 5th order polynomial parameter definition. The results were obtained from MATLAB and Ansys Fluent at different C-rates (0.1 C, 0.2 C and 0.5 C)

4.3 Look-up Table

The MATLAB ode15 s solver does not readily support changing of parameters which are defined through other means than through a function. So, in this case, only the results obtained from Ansys Fluent are investigated. Here in this case (Fig. 6), the discharge curves possess all of the characteristics observed by experimental findings. For 0.1 C it is possible to notice a slight indication of a high voltage plateau. The low-voltage plateau is situated at 2.05 V. The total discharge time is 32 500 s (9.03 h), while the inflection point with the voltage of 2 V occurred at 6 600 s. For higher C-rates even the indication of a higher-voltage plateau disappeared, which is consistent with [13]. For 0.2 C the low-voltage plateau was situated at 2 V and the total discharge time was 16 000 s (4.4 h), while the inflection point with the voltage of

1.89 V occurred at 2 900 s. For 0.5 C the low-voltage plateau was very short and was situated at around 1.85 V. The total discharge time was 6 380 s (1.8 h) and the inflection point with the voltage of 1.65 V occurred at 1 330 s.

The presented results (Fig. 6) were compared to the work of Stroe et al. [13], who used the same type of 3.4 Ah Li-S pouch battery manufactured by OXIS Energy. The nominal voltage of the battery was 2.05 V, the maximum 2.45 V and a minimum of 1.5 V. The ECM has been implemented in MATLAB/Simulink and consisted of one serial resistor and three R-CPE elements. The simulations were carried for 0.1 C, 0.2 C and 0.5 C at 25 ºC. The results were also compared with the experimental measurements.

The shapes of discharge characteristics are generally in agreement for all C-rates. For 0.1 C the discharge curve is the most similar, the only difference was in the time occurrence of the inflection point (9 000 s compared to 6 600 s), while the voltage at that point stayed the same. Slight differences could be found for discharge characteristics at 0.2 C and 0.5 C rates. For the 0.2 C there was a minimal difference between the low-voltage plateaus, while the total discharge time (around 14 000 s compared to 16 000 s) and the time of the inflection point (around 5 000 s compared to 2 900 s) were different. For 0.5 C the main difference was in the total discharge time (slightly under 5 000 s compared to 6 380 s).

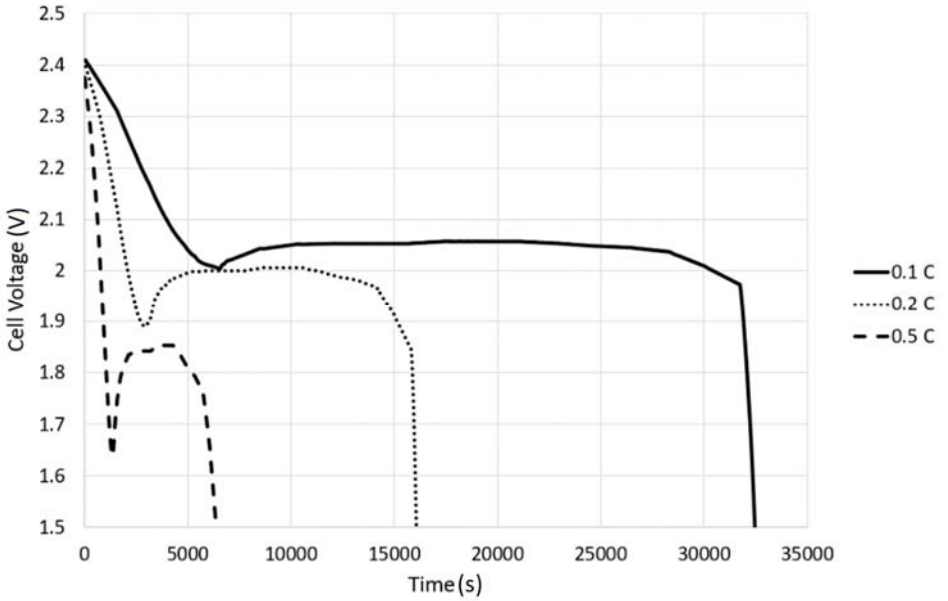

Fig. 6 Simulated discharge curves with the look-up table parameter definition. The results were obtained only from Ansys Fluent at different C-rates (0.1 C, 0.2 C and 0.5 C)

These discrepancies are caused by the different ECMs used here and in the work of Stroe et al [13]. Additionally, Li-S battery parameters show a great temperature dependence, so even a 5 ºC difference might affect the results. It was also noted that in the model of Stroe et al. [13] the inability of a precise determination of the voltage near the inflection point resulted in a considerable source of inaccuracies.

It is also possible to observe a slight drawback of using the look-up table definition. As the look-up table can contain only up to 20 values, certain areas can be

described insufficiently, which is noticeable especially at the end of the discharge. Additionally, the results suggest that Ansys Fluent connect these values through piecewise linear approximation. This is clearly visible at the end of the discharge curves, in which the curve changes suddenly and has a linear character. However, this approximation should not decrease the accuracy of the solution.

Fig. 7 shows the potential distribution at the beginning, in the middle (0.5 SoC) and at the end of the discharge at the positive and the negative current collectors. A potential gradient is visible near the tabs, which might suggest an area of maximum heat generation. During the discharge only the potential at the positive current collector changes, as the boundary condition of 0 V was set to the negative tab, while the defined C-rate was set to the positive tab.

4.4 Using the Implemented Model in Practice

The use of these models is important in terms of the possibility of calculating the temperature fields that arise when charging and discharging these types of batteries. Proper temperature management is then important to set the appropriate operating temperature conditions for the battery. Frequent thermal cycling over a high temperature range can lead to an internal short circuit in the battery (it can be caused by dendritic crystal growth in the internal structure of the battery), or to a thermal runaway phenomenon when exothermic reactions are triggered inside the battery that cause self-heating. In this case, the temperature in the battery exceeds the safe limits many times over, which leads to the total destruction of the battery, or the entire device. These tests are very difficult to implement in practice (in terms of safety and complex equipment) and therefore the use of computer simulation seems to be the best way.

In the experiments mentioned above, the modified model from FLUENT was compared with the empirical model from MatLab in terms of computational algorithm quality. Below is a comparison with a real experiment on a real battery. The tested lithium battery had a capacity of 865 mAh/g. To obtain the data for the ECM model, galvanostatic cycling was performed, where the charging and discharging cycle had a value of 0.1 C and Electrochemical Impedance Spectroscopy (EIS) was performed every 20 % of SoC.

Fig. 8 shows the comparison between experimental measurements and numerical simulations for 0.1 C charge and discharge.

The results are shown in capacity per gram of the active material. Discharge and charge curves were generally in a good agreement. Numerical simulations were able to capture the characteristics such as two voltage plateaus (2.4 V and 2.1 V) and the dip between them. The main difference could be found at the beginning and at the end of the discharge/charge. The sudden change at the beginning of the discharge is very difficult to measure experimentally, as the voltage changes drastically over a very small change in SoC. The difference at the end of the discharge/charge was caused by small number of measurements.

DOI 10.3849/aimt.01525

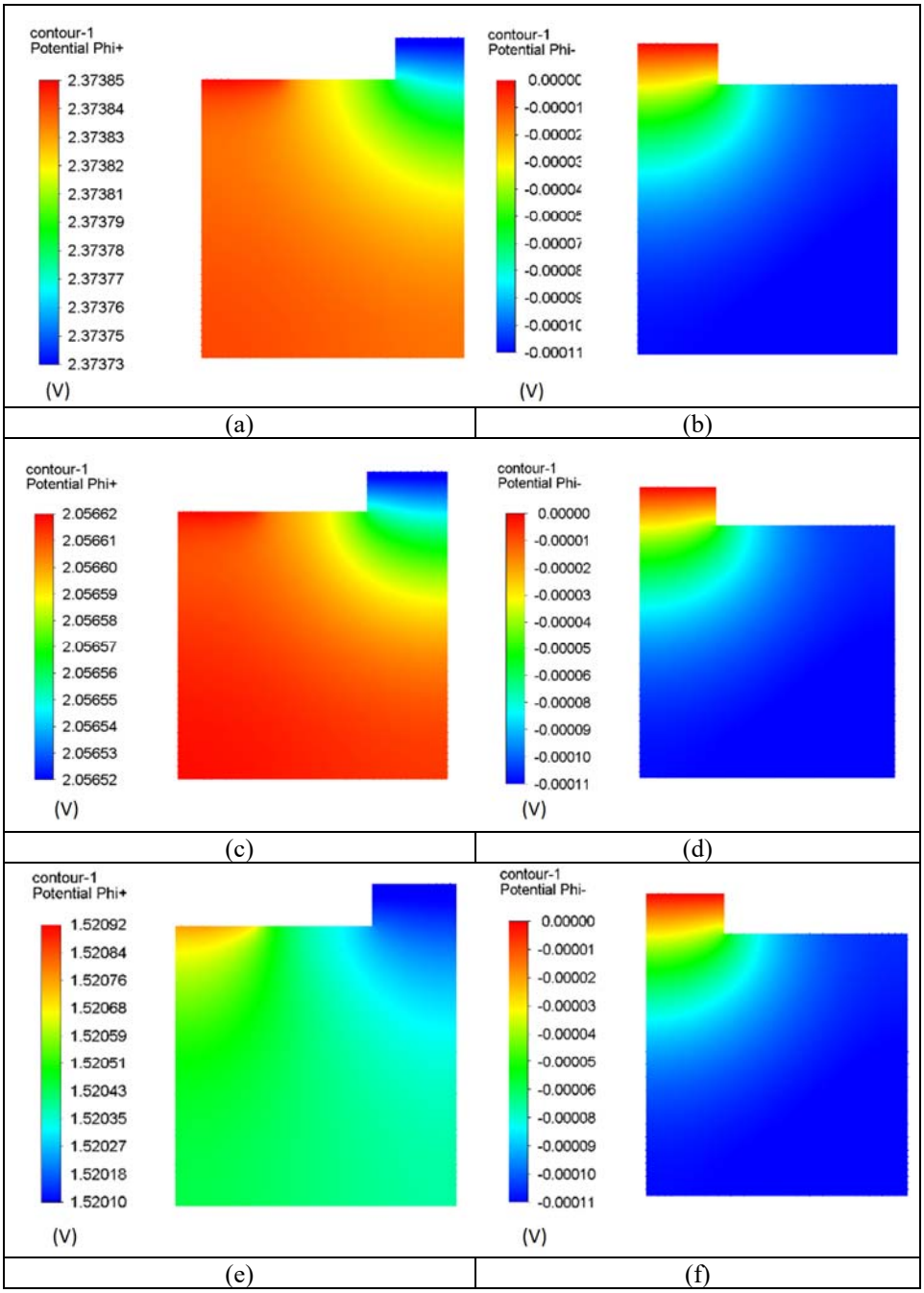

Fig. 7 Illustrations of potential distribution for the positive current collector (Phi+) and the negative current collector (Phi−). The distribution at the beginning of the discharge is shown in (a) and (b). The distribution for 0.5 *SoC is shown in (c) and (d). The distribution at the end of the discharge is shown in (e) and (f)*

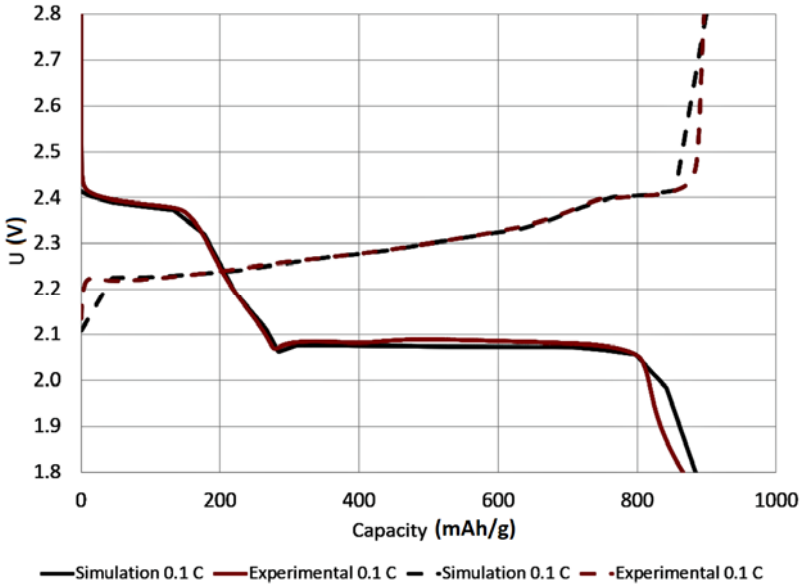

Fig. 8 Example of comparison of experimental measurements and simulations for 0.1 C *for real battery. Dark red curves represent experimental measurements while black curves represent numerical solutions*

5 Conclusions

In this work, a 3D numerical model of a Li-S battery using a commercially available software Ansys Fluent add-on MSMD battery module has been presented. This model was used to model discharge characteristics of a 3.4 Ah Li-S cell. The electrochemical behavior was described using a 1 R-C ECM. The look-up table definition of the ECM parameters allows for the description of complex SoC dependencies as the values are not restricted by any fitting function. As a result, this description can be used for any battery technology, not just for Li-Ion batteries. In comparison to commonly used stand-alone 0D ECMs, the 3D MSMD model is able to study macroscopic effects such as electric potential distribution or temperature distribution in the battery, while keeping the simulation simple, fast and accurate. This could accelerate the implementation of the technology in military applications as it would be possible to study multi-physical effects, which is not possible with the current 0D models. Based on the heating or mechanical deformations, it would be possible to optimize the design of any mobile equipment or to design safe and secure stationary energy storage systems. It would also allow for a better optimization and faster integration of this technology in aircrafts or heavy electric vehicles. The future research will focus on implementing the heat effects to create a complex multi-physical model.

Acknowledgement

This work was supported by the specific graduate research of the Brno University of Technology No. FEKT-S-20-6206.

References

[1] LUCCHESE, F.C., L.N. CANHA, W.S. BRIGNOL, C.A.S. RANGEL, B.K. HAMMERSCHMITT and C.C. CASTRO. A Review on Energy Storage Systems and Military Applications. In: *2020 55th International Universities Power Engineering Conference (UPEC)*. Turin: IEEE, 2020. DOI 10.1109/UPEC49904.2020.9209892.

[2] NXUMALO, Z.C, P. TARWIREYI and M.O ADIGUN. Lithium-Based Batteries in Tactical Military Applications: A review. In: *2015 International Conference on Computer, Communications, and Control Technology (I4CT)*. Kuching: IEEE, 2015, pp. 575-579. DOI 10.1109/I4CT.2015.7219644.

[3] HOFMANN, A.F., D.N. FRONCZEK and W.G. BESSLER. Mechanistic Modeling of Polysulfide Shuttle and Capacity Loss in Lithium–Sulfur Batteries. *Journal of Power Sources*, 2014, **259**, pp. 300-310. DOI 10.1016/j99.jpowsour.2014.02.082.

[4] XU, R., I. BELHAROUAK, X. ZHANG, R. CHAMOUN, C. YU, Y. REN, A. NIE, R. SHAHBAZIAN-YASSAR, J. LU, J.C.M. LI and K. AMINE. Insight into Sulfur Reactions in Li–S Batteries. *ACS Applied Materials & Interfaces*, 2014, **6**(24), pp. 21938-21945. DOI 10.1021/am504763p.

[5] ROBINSON, J.B. et al. 2021 Roadmap on Lithium Sulfur Batteries. *Journal of Physics: Energy*, 2021, **3**(2021), 031501. DOI 10.1088/2515-7655/abdb9a.

[6] DÖRFLER, S., S. WALUS, J. LOCKE, A. FOTOUHI, D.J. AUGER, N. SHATERI, T. ABENDROTH, P. HÄRTEL, H. ALTHUES and S. KASKEL. Recent Progress and Emerging Application Areas for Lithium–Sulfur Battery Technology. *Energy Technology*, 2021, **9**(1). DOI 10.1002/ente.202000694.

[7] DENG, Z., Z. ZHANG, Y. LAI, J. LIU, J. LI and Y. LIU. Electrochemical Impedance Spectroscopy Study of a Lithium/Sulfur Battery: Modeling and Analysis of Capacity Fading. *Journal of The Electrochemical Society*, 2013, **160**(4), pp. A553-A558. DOI 10.1149/2.026304jes.

[8] FOTOUHI, A., D.J. AUGER, K. PROPP, S. LONGO and M. WILD. A Review on Electric Vehicle Battery Modelling: From Lithium-Ion toward Lithium–Sulphur. *Renewable and Sustainable Energy Reviews*, 2016, **56**, pp. 1008-1021. DOI 10.1016/j.rser.2015.12.009.

[9] FOTOUHI, A., D.J. AUGER, K. PROPP and S. LONGO. Electric Vehicle Battery Parameter Identification and SOC Observability Analysis: NiMH and Li-S Case Studies. *IET Power Electronics*, 2017, **10**(11), pp. 1289-1297. DOI 10.1049/iet-pel.2016.0777.

[10] KNAP, V., D.-I. STROE, R. TEODORESCU, M. SWIERCZYNSKI and T. STANCIU. Electrical Circuit Models for Performance Modeling of Lithium-Sulfur Batteries. In: *2015 IEEE Energy Conversion Congress and Exposition (ECCE)*. Montreal: IEEE, 2015, pp. 1375-1381. DOI 10.1109/ECCE.2015.7309853.

[11] KNAP V., D.-I. STROE, R. TEODORESCU, M. SWIERCZYNSKI and T. STANCIU. Comparison of Parametrization Techniques for an Electrical Circuit Model of Lithium-Sulfur Batteries. In: *2015 IEEE 13th International Conference on Industrial Informatics (INDIN)*. Cambridge: IEEE, 2015, pp. 1278-1283. DOI 10.1109/INDIN.2015.7281919.

[12] PROPP, K., M. MARINESCU, D.J. AUGER, L. O'NEILL, A. FOTOUHI, K. SOMASUNDARAM, G.J. OFFER, G. MINTON, S. LONGO, M. WILD and V. KNAP. Multi-Temperature State-Dependent Equivalent Circuit Discharge Model for Lithium-Sulfur Batteries. *Journal of Power Sources*, 2016, **328**, pp. 289-299. DOI 10.1016/j.jpowsour.2016.07.090.

[13] STROE, D.-I., V. KNAP, M. SWIERCZYNSKI and E. SCHALTZ. Electric Circuit Modeling of Lithium-Sulfur Batteries During Discharging State. In: *2017 IEEE Energy Conversion Congress and Exposition (ECCE)*. Cincinnati: IEEE, 2017, pp. 1024-1029. DOI 10.1109/ECCE.2017.8095899.

[14] LI, G. and S. LI. Physics-Based CFD Simulation of Lithium-Ion Battery under the FUDS Driving Cycle. *ECS Transactions*, 2015, **64**(33), pp. 1-14. DOI 10.1149/06433.0001ecst.

[15] JUNG, S. and D. KANG. Multi-Dimensional Modeling of Large-Scale Lithium-Ion Batteries. *Journal of Power Sources*, 2014, **248**, pp. 498-509. DOI 10.1016/j.jpowsour.2013.09.103.

[16] YAZDANPOUR, M., P. TAHERI, A. MANSOURI and B. SCHWEITZER. A Circuit-Based Approach for Electro-Thermal Modeling of Lithium-Ion Batteries. In: *2016 32nd Thermal Measurement, Modeling & Management Symposium (SEMI-THERM)*. San Jose: IEEE, 2016, pp. 113-127. DOI 10.1109/SEMI-THERM.2016.7458455.

[17] CHEN, M. and G.A. RINCON-MORA. Accurate Electrical Battery Model Capable of Predicting Runtime and I–V Performance. *IEEE Transactions on Energy Conversion*, 2006, **21**(2), pp. 504-511. DOI 10.1109/TEC.2006.874229.

[18] VYROUBAL, P. and T. KAZDA. Equivalent Circuit Model Parameters Extraction for Lithium Ion Batteries Using Electrochemical Impedance Spectroscopy. *Journal of Energy Storage*, 2018, **15**, pp. 23-31. DOI 10.1016/j.est.2017.10.019.

[19] SØRENSEN, K., N. HOUBAK and T. CONDRA. Solving Differential–Algebraic Equation Systems by Means of Index Reduction Methodology. *Simulation Modelling Practice and Theory*, 2006, **14**(3), pp. 224-236. DOI 10.1016/j.simpat.2005.05.002.

[20] SHAMPINE, L.F. and M.W. REICHELT. The MATLAB ODE Suite. *SIAM Journal on Scientific Computing*, 1997, **18**(1), pp. 1-22. DOI 10.1137/S1064827594276424.